HTML ABSTRACT + LINKS

Electrofreezing of confined water

Ronen Zangi[a] and Alan E. Mark
The Groningen Biomolecular Sciences and Biotechnology Institute, Department of Biophysical Chemistry, University of Groningen, Nijenborgh 4, 9747 AG Groningen, The Netherlands

(Received 15 December 2003; accepted 23 January 2004)

We report results from molecular dynamics simulations of the freezing transition of TIP5P water molecules confined between two parallel plates under the influence of a homogeneous external electric field, with magnitude of 5 V/nm, along the lateral direction. For water confined to a thickness of a trilayer we find two different phases of ice at a temperature of $T=280$ K. The transformation between the two, proton-ordered, ice phases is found to be a strong first-order transition. The low-density ice phase is built from hexagonal rings parallel to the confining walls and corresponds to the structure of cubic ice. The high-density ice phase has an in-plane rhombic symmetry of the oxygen atoms and larger distortion of hydrogen bond angles. The short-range order of the two ice phases is the same as the local structure of the two bilayer phases of liquid water found recently in the absence of an electric field [J. Chem. Phys. **119**, 1694 (2003)]. These high- and low-density phases of water differ in local ordering at the level of the second shell of nearest neighbors. The results reported in this paper, show a close similarity between the local structure of the liquid phase and the short-range order of the corresponding solid phase. This similarity might be enhanced in water due to the deep attractive well characterizing hydrogen bond interactions. We also investigate the low-density ice phase confined to a thickness of 4, 5, and 8 molecular layers under the influence of an electric field at $T=300$ K. In general, we find that the degree of ordering decreases as the distance between the two confining walls increases. © *2004 American Institute of Physics.* [DOI: 10.1063/1.1687315]

I. INTRODUCTION

Frozen water in forms ranging from snowflakes to icebergs has fascinated scientists for centuries. Ice exhibits a rich polymorphism of phases that are built of tetrahedrally coordinated hydrogen-bonded water molecules.[1] In hexagonal, I_h, and cubic, I_c, ice phases the tetrahedral geometry is nearly perfect. The hexagonal ice, however, is the most stable form of ice at ambient pressure except for a small region of low temperatures (-150 to -120 C).[2]

The transformation of liquids into crystals in a three dimensional system is a first-order phase transition. Thus, the crystalline phase emerges abruptly from the liquid phase. In the absence of a foreign surface or particle to promote heterogeneous nucleation, this phase transition begins with the spontaneous nucleation of molecules into small aggregates which, if they reach a critical size, form the seeds for the new phase. For this reason, pure water, even if cooled down to 30 °C below its freezing point, can not generate stable nuclei on which ice can grow.

One way to increase the rate of formation of stable nuclei is by the application of an electric field. When a sample of a polar liquid is exposed to an external electric field it undergoes polarization. At small electric fields the polarization is linearly proportional to the applied field. The proportionality constant is a measure of the dielectric constant of the sample. At high electric fields, deviations from linearity occur and the polarization eventually saturates. This behavior for the case of bulk liquid water has been observed experimentally[3] and computationally.[4–8] It is found that the polarization curve fits well to the classical Langevin function. Thus, at high field strengths the polarization becomes constant and the resulting dielectric constant falls to unity. The favorable energetic interaction of the electric field with the dipole moment of the molecules reduces the entropy of the liquid phase due to the restriction of the orientational degrees of freedom along axes perpendicular to the applied field. Therefore, the difference of the entropic contribution to the free energy between the liquid phase and the solid phase diminishes. In this case, if the entropy reduction is large enough and the interactions between the molecules are strong, the most stable phase would correspond to the crystalline phase.

This phenomenon was demonstrated by Gavish *et al.*[9] They studied substrate nucleation of water by polar and nonpolar amino acid crystals that have no match at all with the crystal structure of ice. They found that the crystals that have a polar axis induce freezing at temperatures 3–5 °C higher than the crystals that do not have a polar axis. They interpreted their finding in terms of an electric field mechanism that helps align the water molecules into a proton ordered, polar along its hexagonal axis, ice nucleus. Although they attributed the change in the freezing temperature to be kinetic in origin, Wilen[10] offered a thermophysical explanation for the observed behavior which predicts an elevation of the equilibrium freezing temperature. The significance of the results is that an electric field mechanism may be of general

[a]Author to whom correspondence should be addressed. Electronic mail: r.zangi@chem.rug.nl

 © 2004 American Institute of Physics

Downloaded 01 Apr 2004 to 129.125.42.3. Redistribution subject to AIP license or copyright, see http://jcp.aip.org/jcp/copyright.jsp

applicability for ice nucleation and could also operate in other known ice nucleators such as silver iodide.

In computer simulation, upon reducing the temperature, phase trajectories tend to become trapped into a region of metastable glassy states.[11] The glassy state prevents, within the time scale of a typical simulation, a spontaneous homogenous nucleation of ice. However, due to the promotion of freezing under the action of an electric field, several computational studies, have reported spontaneous freezing of bulk liquid water.

Svishchev and Kusalik[12,13] studied electrofreezing of supercooled liquid water. They found that for a field with strength of 5 V/nm TIP4P water, at 250 K, undergoes crystallization to cubic ice. They also found at temperatures of 225–240 K and at 3–5 kbar that the homogenous electric field induces the formation of a previously unknown polymorph of ice which they denote ice XII.[14] Following these observations, similar results were obtained in later studies.[15–18] In earlier studies Watanabe *et al.*[6] examined the effect of an external electric field on liquid water between two conducting plates. They found evidence for the existence of two distinct continuous phase transitions. Depending on its strength, an electric field can weaken or destroy the hydrogen bonding network.[19] The anomalous behavior of the polarization with an increase in temperature observed in a medium-sized water cluster has been attributed to an interplay between the water–water interactions and the interaction of the electric field with the water molecules.[20,21]

The strong electric field applied in computational studies accelerates the process of homogenous nucleation which in many cases would otherwise far exceed typical simulation times. Field strength of ~ 5 V/nm are comparable to that experienced by water molecules within molecular distances from the surfaces of certain types of biopolymers,[22] to the fields generated by cracks in crystals[9] and are within the operating range of lasers.

Experimental studies also indicate that confinement of many liquids to films thinner than 4–6 molecular layers promote solidification.[23–25] This is because the entropy of the liquid phase is decreased due to the restricted motion of the particles in the transverse direction. In recent molecular dynamics simulations it was found that water confined to a slab geometry can freeze at ambient conditions.[26,27] Since the tetrahedral arrangement of water is incompatible with a two-dimensional geometry the ice phases found are stable only for a small range of plate separations that enable the optimal formation of hydrogen bonds. The structure that was found for monolayer ice[26] and bilayer ice[27] had a rhombic in-plane symmetry of the oxygen atoms and the hydrogen positions were ordered. However, above the thickness of a bilayer, the degree of which the solid phase is enhanced due to confinement were found to be insufficient to freeze liquid water at ambient conditions.[27] In this paper we investigate the freezing transition of water confined to a thickness of 3–8 layers under the action of an external electric field acting in the direction parallel to the confining walls. For water confined to a thickness of a trilayer we find two different phases of ice at a temperature of $T=280$ K. The low-density ice phase is built from hexagonal rings parallel to the confining walls and corresponds to the structure of cubic ice. The high-density ice phase has an in-plane rhombic symmetry of the oxygen atoms and larger distortions of the hydrogen bond angles. The short range order of the two ice phases is the same as the local structure of the two bilayer phases of liquid water found previously in the absence of an electric field.[27] These high- and low-density phases of water differ in local ordering at the level of the second shell of nearest neighbors. The results reported in this paper, show a close similarity between the local structure of the liquid phase and the short range order of the corresponding solid phase. This similarity might be enhanced in water due to the deep attractive well characterizing hydrogen bond interactions. We also investigate the low-density ice phase confined to a thickness of 4, 5, and 8 molecular layers under the influence of an electric field at $T=300$ K. In general, we find that the degree of ordering decreases as the distance between the two confining walls increases.

II. METHODS

The MD simulations were performed using the GROMACS package version 3.1.[28] The time step used for integrating Newton's equations of motion was 0.002 ps. All simulations were performed using a constant number of particles and a fixed volume. Each system was coupled to a thermal bath[29] using a coupling time of 0.1 ps. The evaluation of the nonbonded interactions was performed using a twin range cutoff of 0.9 and 1.4 nm. Interactions within the shorter cutoff were updated every step while longer range interactions were updated every five steps. To account for the neglect of electrostatic interactions beyond the long range cutoff a reaction-field correction[30] assuming a relative dielectric constant of 78.0 was applied.

The five-site, tetrahedrally coordinated, TIP5P model[31] was used to describe the water molecules. The TIP5P water model was chosen because it represents the electron lone pair sites explicitly. This favors formation of colinear angles of the hydrogen bonds. Note, that the magnitude of the hydrogen bond interactions is insufficient to cause rehybridization of the sp^3 hybridized oxygen atom of water which could results in a change in either the molecular H–O–H angle or in the spatial distribution of the electron lone pairs.[1,32] Therefore, it is expected that in confined geometries the tetrahedral molecular arrangement of the water molecules is preserved and the degree of the hydrogen bond distortion (from a colinear angle) would be in the range of the distortions found in the high-pressure bulk ice phases. The O–H bond lengths and the H–O–H bond angle were constrained using the SETTLE algorithm.[33] The lone pair electrons were treated as dummies (virtual) atoms. Their positions are computed as a function of the oxygen and the hydrogen positions. The forces acting on the dummy atoms were distributed over the atoms which were treated explicitly. In this way, the total energy and the total angular momentum of the system are conserved.[34]

A system of 1200 water molecules was placed between two walls with a triangular arrangement of atoms out-of-registry with respect to one another. The positions of the monolayer of atoms within the walls were constrained to a

Downloaded 01 Apr 2004 to 129.125.42.3. Redistribution subject to AIP license or copyright, see http://jcp.aip.org/jcp/copyright.jsp

lattice spacing of 0.23 nm. Periodic boundary conditions were imposed only in the x and y directions. The water–wall interactions were represented by a 6-12 Lennard-Jones (LJ) potential with the parameters: $\sigma_{(O_w-W)}=0.316$ nm, $\sigma_{(H_w-W)}=0.284$ nm and $\epsilon_{(O_w-W)}=0.831$ kJ/mol, $\epsilon_{(H_w-W)}=0.415$ kJ/mol. These parameters represent approximately the van der Waals (vdW) interaction between a water molecule and a quartz (SiO_2) surface. A weighted average of silicon and oxygen atom parameters, taken from the GROMOS96 force field,[35] was used in a geometric combination rule together with TIP5P parameters. The simulations pertain, therefore, only to confinements due to surfaces where the interactions with the water molecules are weaker than hydrogen bonding interactions. Since the LJ parameters of the TIP5P water hydrogen are equal to zero, $\sigma_{(H_w-W)}$ was estimated from the ratio of the vdW radius between oxygen and hydrogen.[36] The value of $\epsilon_{(H_w-W)}$ was taken as half the corresponding value associated with oxygen. There was no interaction between the two lone-pair sites of water and the wall.

The wall separation, H, was derived from the distance, d, between the fixed center of mass of the surface atoms of the two walls. To calibrate the values of H, we estimated a reference value of the wall separation, H_0, by using the transverse density distribution of the center of mass of the oxygen atoms at a simulation point taken from a previous study that corresponded to a bilayer of liquid water, $d_0=0.82$ nm.[26] This distribution exhibited a sharp curve against the wall and, therefore, provided a precise determination of the length along the z direction that the center of mass of the oxygen atoms occupied. To this value, the diameter of a water oxygen atom was added yielding $H_0=0.58$ nm. The value of the wall separation, H_x, for simulation that was performed at d_x was estimated by $H_x=H_0+(d_x-d_0)$.

The value of the area of the simulation box in the xy plane, A, was used to vary the density of the water molecules at constant plate separation, thus, generating lateral compression or expansion. In the calculations of the radial distribution function, the normalizing volume element was taken to be cylindrical in accordance with the system geometry. The cutoff distance used to assign the presence of a hydrogen bond was taken as the distance to the minimum between the first and the second peaks of the oxygen–hydrogen pair correlation function in the different phases. This yielded a cutoff value of 0.242 nm.

The force acting on a water molecule due to the action of the external electric-field is given by

$$\vec{F}_{w-ef}=\sum_k q_k\cdot\vec{E}. \tag{1}$$

The sum in Eq. (1) is over the $k=4$ charged sites of the TIP5P model; the two hydrogen atoms and the two lone-pair electrons. The electric field, $\vec{E}$, was taken to be static and uniform. Its vector components were chosen to be nonzero only along the y axis, a direction parallel to the confining walls. The amplitude of the electric field was taken to be 5.0 V/nm. Due to the difficulty in observing spontaneous homogenous nucleation in molecular liquids on the time scale applicable to computational studies, the thermodynamic conditions that are used are more drastic than those that are used normally in experiments.

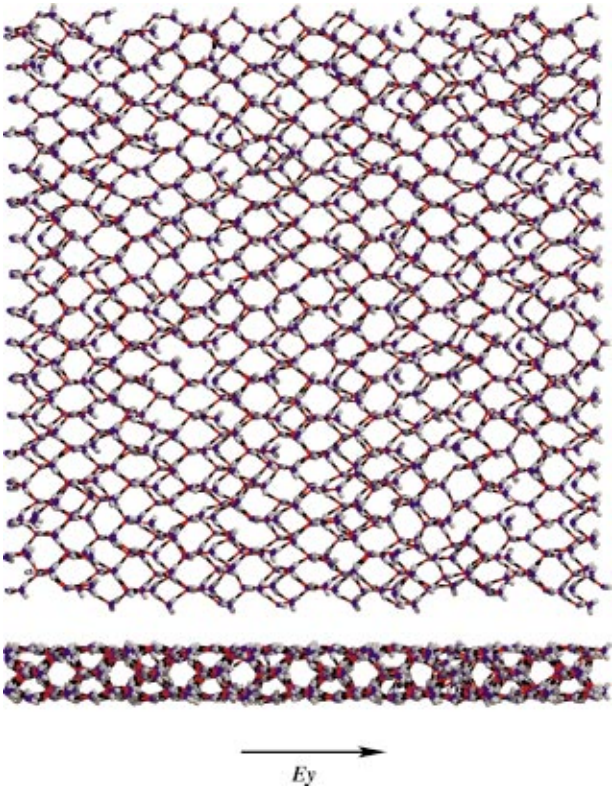

FIG. 1. (Color) Instantaneous configuration of the lateral and transverse structure of confined ice ($H=0.92$ nm) obtained at $A=46.24$ nm^2 and $T=280$ K under the action of an applied electric field along the y axis. Oxygen atoms are depicted in blue, hydrogen atoms in gray, and the lone pair electron sites in red.

The initial configuration of each simulation at a different value of H was taken from a corresponding equilibrated box of TIP5P water molecules in the liquid phase without the action of an electric field at $T=300$ K and with a lateral pressure coupling of 1 bar.[27] The system was then equilibrated for at least 16 ns and then data was collected every 10 ps for an additional 4 ns.

III. RESULTS

In the simulations of confined liquid water under the influence of an external electric field along the lateral direction we observed crystallization at certain values of plate separations. The structure of ice obtained after 20 ns for a plate separation of $H=0.92$ nm, area $A=46.24$ nm^2, and a temperature of $T=280$ K is shown in Fig. 1. The confining parameter of $H=0.92$ nm generates ice with a thickness of three layers (see Fig. 2). The in-plane structure of the hydrogen bonding network forms hexagonal rings. However, these rings are not built by water molecules present in the same plane, as reported by Koga *et al.* for the case of bilayer ice,[37] but involve water molecules of the middle layer as well. This is clearly shown in the out-of-plane structure. The hexagonal

Downloaded 01 Apr 2004 to 129.125.42.3. Redistribution subject to AIP license or copyright, see http://jcp.aip.org/jcp/copyright.jsp

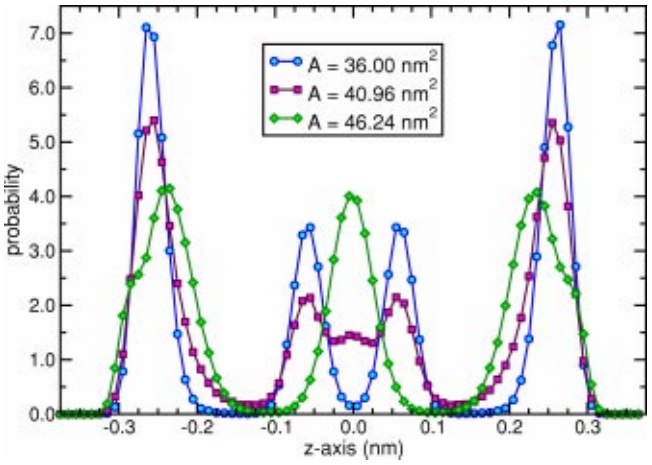

FIG. 2. Normalized distribution of the center of mass of oxygen atoms along the transverse direction for $A=36.0$, 40.96, and 46.24 nm^2 ($H=0.92$ nm and $T=280$ K).

packing of the oxygen atoms corresponds to the cubic ice phase. However, the rings are elongated along the y axis, the direction of the applied electric field. The layer next to both surfaces is slightly disrupted due to the incompatibility of a tetrahedral arrangement with a flat surface that does not participate in the hydrogen bonding network. As a consequence, the transverse density profile of these outer layers is split. This is shown in Fig. 2 as shoulders on the main outer peaks.

The ice configuration shown in Fig. 1 was laterally compressed. Figures 3 and 4 show the structures obtained at $A=40.96$ and 36.0 nm^2, respectively. It is clear that the structure of ice at $A=36.00$ nm^2 is different from the one at $A=46.24$ nm^2. The in-plane symmetry of all three layers is

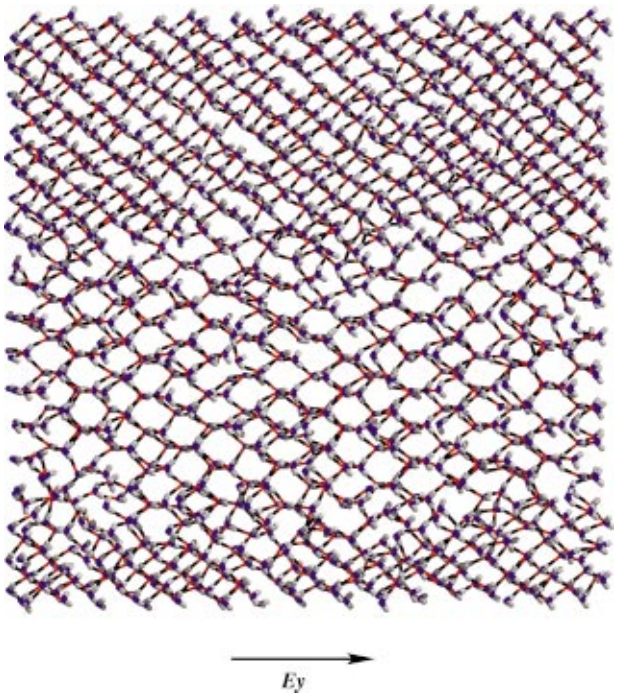

FIG. 3. (Color) Instantaneous lateral configuration obtained at $A=40.96$ nm^2 showing a coexistence between two different ice structures. Color code is the same as in Fig. 1.

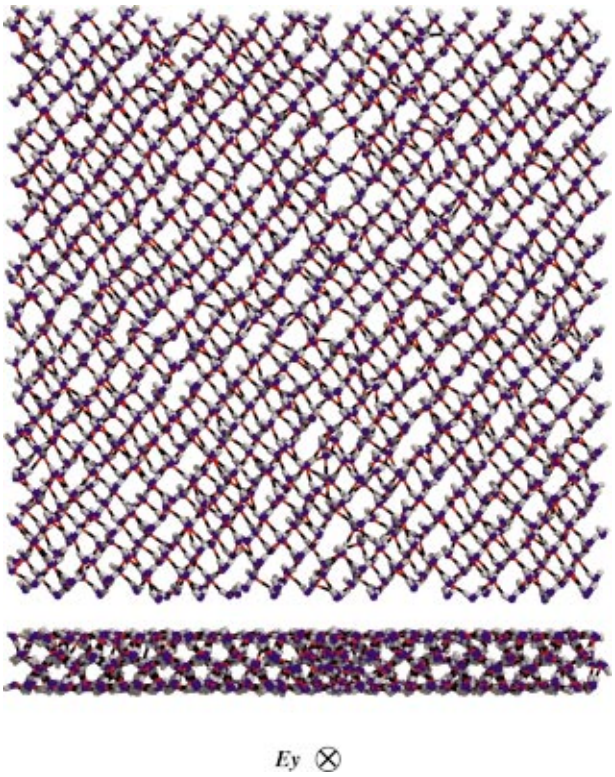

FIG. 4. (Color) Instantaneous configuration of the lateral and transverse (the y axis points inward relative to the paper plane) structure of ice obtained at $A=36.0$ nm^2 under the action of an applied electric field along the y axis. The transverse structure was rotated by 2° about the z axis to provide a clear view of the arrangement of the atoms.

rhombic, the same as the in-plane structure of the monolayer[26] and the bilayer[27] ice phases found in the absence of an electric field. This is easily revealed by the pair correlation function of the oxygen atoms displayed in Fig. 5. The curve for $A=36.0$ nm^2 exhibits a second maximum, due to the second shell of nearest neighbors, at around $r=0.37$ nm. In contrast, the curve for $A=46.24$ nm^2 has a minimum at $r=0.37$ nm. Similar observations were made in

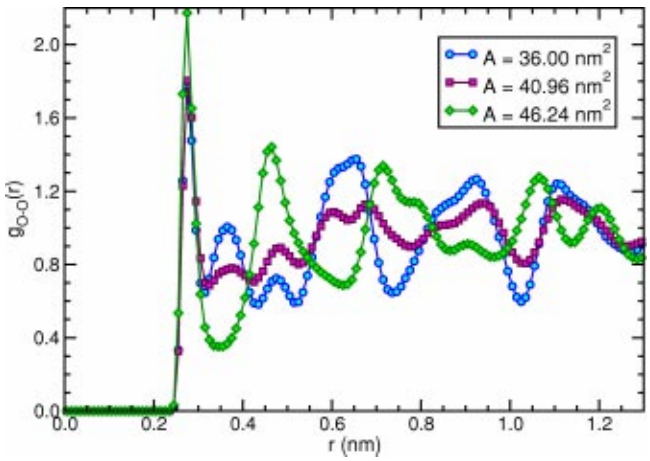

FIG. 5. The oxygen–oxygen pair correlation function for the two phases of ice found at $A=46.24$ and 36.0 nm^2 that are shown in Figs. 1 and 4, respectively. Also plotted is the pair correlation function for a system of these phases in coexistence, $A=40.96$ nm^2, shown in Fig. 3.

Downloaded 01 Apr 2004 to 129.125.42.3. Redistribution subject to AIP license or copyright, see http://jcp.aip.org/jcp/copyright.jsp

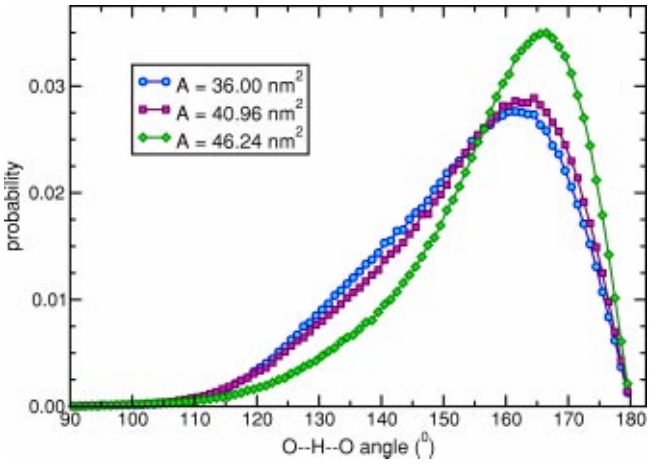

FIG. 6. Normalized distribution of the hydrogen-bond angles (donor–hydrogen–acceptor) for the systems analyzed in Figs. 2 and 5.

experimental x-ray and neutron scattering studies of the structure of water confined in a hydrogel,[38] in Vycor glass[39,40] and at a hydrophobic surface.[41] In these studies it was observed that while the first peak in the radial distribution function is not significantly affected due to the restricted geometries, a hump appears at around $r=0.37$ nm in a manner identical to that induced by an increase in pressure.[42] The appearance of this peak was interpreted in terms of the distortion of the hydrogen bonds. Note that the middle layer shown in the transverse density profile of the oxygen atoms in Fig. 2 at $A=36.0$ nm^2 is buckled.[43,44] However, the system corresponds to three layers and not to four layers since the transverse distance between the split peaks of the central layer is much smaller than the oxygen–oxygen radial distance.

Figure 6 shows the normalized distribution of the hydrogen bond angles for the three values of A analyzed above. The curve that corresponds to the ice phase derived from the structure of cubic ice ($A=46.24$ nm^2) has the smallest degree of distortion in the hydrogen bond angles. It is a maximum at an angle of 166°. Although the maximum of the curve that corresponds to the ice phase at $A=36.0$ nm^2 is only slightly shifted to smaller angles (to ~162°), the intensity at the maximum is smaller. There is also a larger population of angles in the range 115°–155° that indicates higher distortions. Indeed all of the bulk ice phases known at higher density (or higher pressure) exhibit distortions of the hydrogen bond angle.[1,2,32] In general the higher the pressure the higher the distortion. In Table I the densities of the ice phases at different values of A are presented. The ice phase that corresponds to the structure of cubic ice ($A=46.24$ nm^2) has a low density, in fact, lower than the density of bulk cubic ice. The ice structure that corresponds to the rhombic in-plane structure, $A=36.0$ nm^2, has a higher density, however, it is still lower than the density of most high-pressure bulk ice phases. The origin of the lower density of the ice phases under confinement may be due to the incompatibility of the tetrahedral network with a slab confinement and/or due to the response of the ice structure to the applied electric field. The later also generates a distortion of the hexagonal rings along the direction of the field. The average number of hydrogen bonds per molecule are also reported in Table I. For the high-density ice phase, each molecule participates, on average, in more hydrogen bonds than for the low-density ice phase. This is because the structure of the layers next to the surface in the low-density ice has an incomplete number of nearest neighbors. Although the high-density ice phase is characterized by a higher number of hydrogen bonds per molecule, the hydrogen bonds in the low density ice phase are less distorted. These effects make opposing contributions to the potential energy of the system, U_{pot}. As shown in Table I, $|U_{\mathrm{pot}}|$ is only slightly larger in the high-density ice phase.

TABLE I. Density, average number of hydrogen bonds and potential energy of confined ice phases induced by an external electric-field with magnitude $|E|=5.0$ V/nm for different plate separations.

H (nm)	# of layers	A (nm^2)	T (K)	ρ (g/ml)	$\langle N_{H\text{-bond}}\rangle$	$\langle U_{\mathrm{pot}}\rangle$ (kJ/mol)
0.92	3	36.0	280	1.09	3.83	−50.5
0.92	3	40.96	280	0.96	3.64	−48.7
0.92	3	46.24	280	0.85	3.61	−49.4
1.14	4	38.40	300	0.82	3.57	−47.8
1.36	5	31.02	300	0.85	3.64	−47.7
1.86	8	23.03	300	0.84	3.64	−46.7

In Fig. 3 the configuration of the confined frozen water for $A=40.96$ nm^2 is shown. It corresponds to a coexistence between the low-density and high-density ice phases with approximately an equal amount of each phase. Thus, the transverse density profile shown in Fig. 2 and the radial distribution function shown in Fig. 5 for this value of A is an average of the corresponding curves of the two ice phases. However, the distribution of the hydrogen bond angles (and so the average number of hydrogen bonds) and the potential energy of the system, $|U_{\mathrm{pot}}|$, are both smaller than what is expected from an average of the values of the two homogeneous phases. The reason is that the interfacial region between the two ice phases, which is relatively large compared to the system size, does not permit an optimal connectivity between the water molecules. Hence, the system with the phase coexistence is characterized by a smaller number of hydrogen bonds and a smaller value of $|U_{\mathrm{pot}}|$. Note that it is not possible to present a clear transverse view as the lattice axis of the two crystals are not aligned with each other.

In Table I results from three other simulations, at $H=1.14$, 1.36, and 1.86 nm that were started from a configuration of the liquid phase and resulted in crystallization due to the application of the electric field, are reported. Crystallization occurs even when the system was coupled to a thermal bath with $T=300$ K. Not every value of plate separation allows freezing, however, we did not perform systematic studies to investigate the range of plate separations that did allow formation of ice. The guiding criterion that we used to find the value of H that supported the formation of the confined ice phases was the value of the transverse pressure. Large positive values of the transverse pressure indicate that a relaxed structure can be obtained upon increasing H while large negative values indicate that a decrease of H is needed.

Downloaded 01 Apr 2004 to 129.125.42.3. Redistribution subject to AIP license or copyright, see http://jcp.aip.org/jcp/copyright.jsp

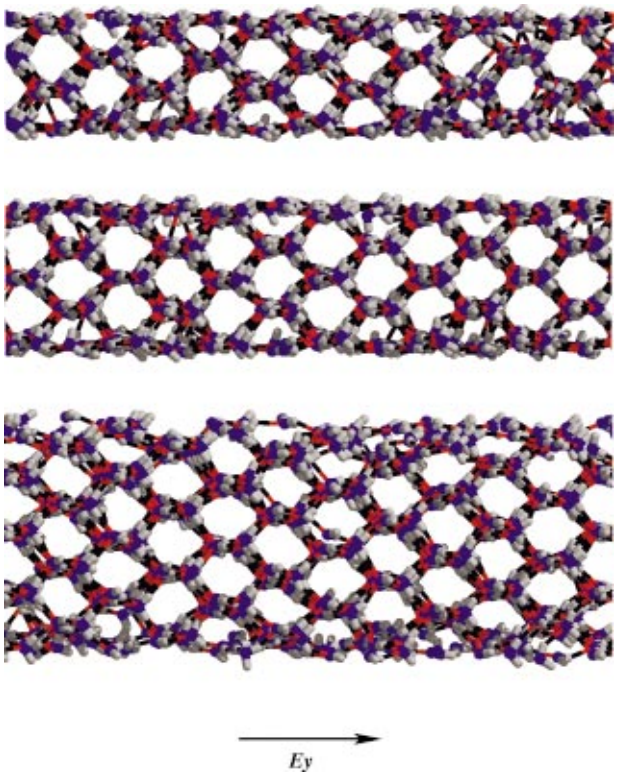

FIG. 7. (Color) Out-of-plane structures of ice induced by the action of an external electric field (along the y axis) at $T=300$ K for three values of wall separation, H. From top to bottom: $H=1.14$, 1.36, and 1.86 nm. Color scheme is the same as in Fig. 1.

The density of the ice phases obtained is similar to the low-density ice phase found at $H=0.92$ nm. In general, it is expected that one would observe a larger number of hydrogen bonds per molecule since the contribution of the interfacial regions to the entire system decreases. This is only partially shown in Table I for $H=1.14$, 1.36, and 1.86 nm. A possible explanation for not observing an increase in the number of $\langle N_{H\text{-bond}}\rangle$ at $H=1.86$ nm compared to $H=1.36$ nm is that as H increases the promotion of solidification due to confinement decreases. This can also explain the decrease of $|U_{\text{pot}}|$ at $H=1.86$ nm compared to that at $H=1.36$ nm. However, the value of $|U_{\text{pot}}|$ is similar for $H=1.14$ nm and $H=1.36$ nm.

Instantaneous configurations along the transverse direction for the simulations at $H=1.14$, 1.36, and 1.86 nm are shown in Fig. 7. The in-plane structure in all cases (data not shown) is the same as that displayed in Fig. 1. The structure corresponds to proton-ordered cubic ice. Even at the largest plate separation studied, the hydrogen-bonding network of the layers next to the surfaces is disrupted. Figure 8 shows the radial distribution function of the oxygen atoms. In general, all three plots are similar and resemble that shown in Fig. 5 for $A=46.24$ nm^2. However, the intensity of the peaks are larger for smaller values of H. This is also evident in the transverse density profile displayed in Fig. 9. Note that resolution of the peaks cannot be deduced from the instantaneous plots displayed in Fig. 7. The simulations at $H=1.14$, 1.36, and 1.86 nm correspond to a thickness of 4, 5, and 8 molecular layers, respectively. There are no secondary splittings

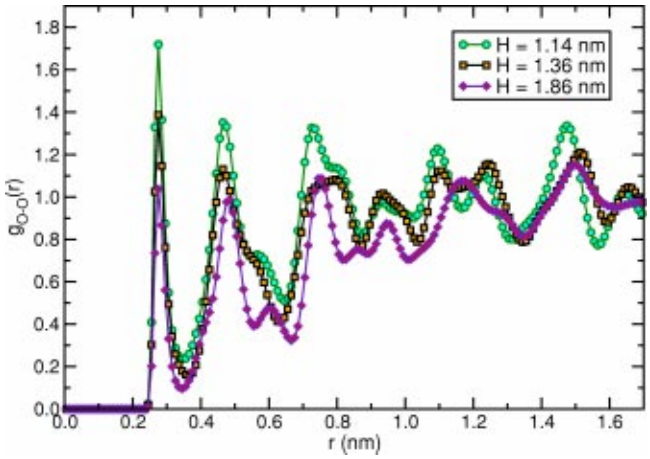

FIG. 8. The oxygen–oxygen pair correlation function for plate separations, $H=1.14$, 1.36, and 1.86 nm.

(buckling) of any of the layers as occurred at $H=0.92$ nm. Figure 10 displays the distribution of the hydrogen-bond angles. Again, the curves are very similar to that observed for the low-density ice phase at $H=0.92$ nm. However, as H increases the distortion of the hydrogen bonds decreases.

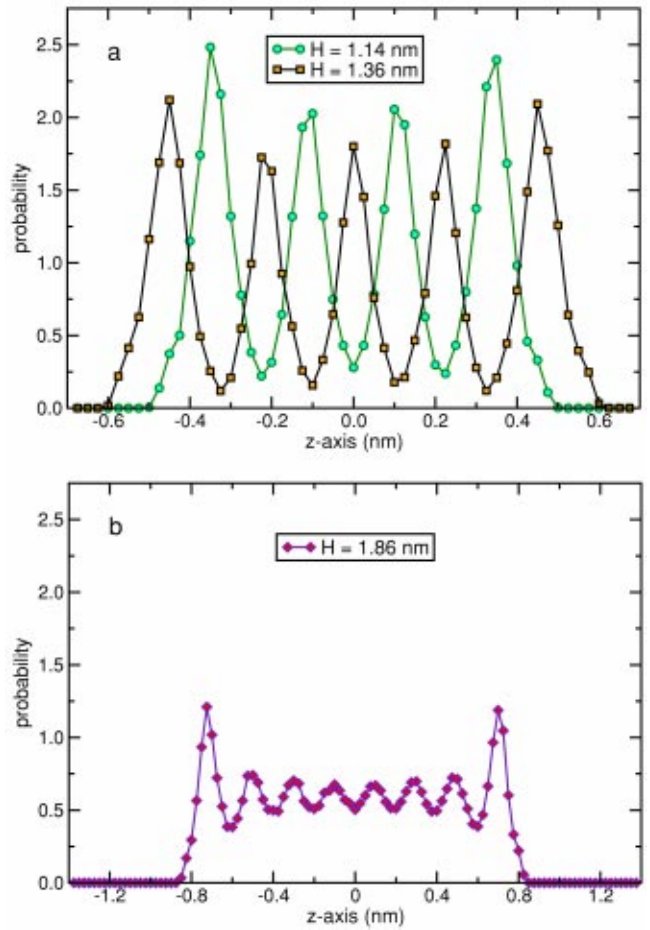

FIG. 9. Normalized distribution of the center of mass of oxygen atoms along the transverse direction for the three values of wall separations shown in Fig. 7: (**a**) $H=1.14$ 1.36 nm and (**b**) $H=1.86$ nm.

Downloaded 01 Apr 2004 to 129.125.42.3. Redistribution subject to AIP license or copyright, see http://jcp.aip.org/jcp/copyright.jsp

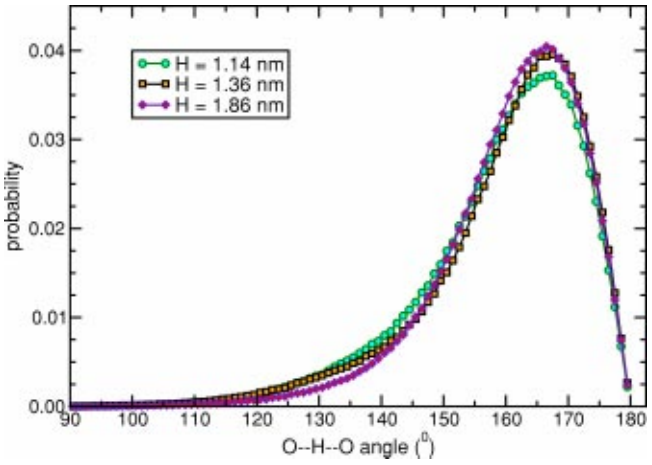

FIG. 10. Normalized distribution of the hydrogen-bond angles (donor–hydrogen–acceptor) for plate separations, $H=1.14$, 1.36, and 1.86 nm.

IV. DISCUSSION

In this paper we have shown that liquid water confined to a slab geometry can be induced to crystallize under the influence of an external electric field along the lateral direction. As was found in the case without an external field, the wall separation plays a crucial role. For example, in the trilayer system no crystallization was observed for $H \leqslant 0.90$ nm after 20 ns equilibration. However, this dependency decreases as the value of the wall separation increases. The promotion of crystallization due to the action of an electric field seems to be thermodynamic in origin. It has been shown experimentally[45,46] and computationally[27] that water confined to thickness of few molecular layers under ambient conditions does not freeze in contrast to other molecular liquids. We interpret the enhanced stability of the ice phases relative to the liquid phase in terms of the reduced entropy of the later. The interaction of the dipoles of the molecules with electric field restrict their orientational degree of freedom around axes perpendicular to the field vector. Thus, the difference of the free energy between the liquid phase and the solid phase decreases and crystallization occurs earlier. The work shows that the synergistic effects of confinement and electric fields can be used in concert to manipulate properties of water, which may have possible applications such as in manipulating solutions within high-density microfluidic chips.[47]

The structure of the ice phases that we observe at low-density corresponds to cubic ice. Under normal conditions liquid water freezes to hexagonal ice. A possible explanation for this is that a parallel arrangement of the molecular dipoles can be supported by the diamond-type packing of cubic ice but not by the hexagonal packing. Therefore, if the applied field is high enough, the cubic arrangement of the system is energetically more favorable.[12]

The transformation of the ice structure with in-plane hexagonal symmetry (low density) to a phase with in-plane rhombic symmetry (high density) is found to be a strong first order transition. Since there is no group–subgroup relation between the two phases the transition must be reconstructive. The strong first order transition observed is due to the deep attractive well of the intermolecular interactions between the water molecules. In hard sphere systems, this transition exhibits intermediate phases with either weak first order or second order character. Addition of an attractive well to the interparticle potential changes the transition to be direct with strong first order character.[48]

Despite the fundamental difference existing between the amorphous structure of the liquid phase and the crystalline structure of the solid phase, it has been argued that this difference is only in the degree of order rather than a qualitative difference.[49] Thus, the solid and the liquid states of matter share the same local (short range) structure. The local structure of the two ice phases that we found in this study is the same as the local structure of the two phases of bilayer of liquid water found in the absence of an external field.[27] The difference between the two liquid phases is in the local ordering at the level of the second shell of nearest neighbors and in the transverse density profile. In both the liquid and the solid phases, the second peak, which gives information about the local arrangement of the oxygen atoms, is shifted at the high-density phases, toward lower values of interparticle separation ($r \sim 0.37-0.41$ nm). In this case, a larger distortion of hydrogen-bond angle is observed. However, the first peak in the radial distribution function is hardly affected by the density increase. This similarity between the local structure of the liquid phase and the short range structure of the solid phase might be stronger in water due to the deep attractive well characteristic to hydrogen bond interactions. In addition, the strong angle dependency of the hydrogen-bonds forces a tetrahedral order of the first shell of nearest neighbors.[50]

A liquid–liquid transition has also been reported in Monte Carlo studies to take place between a bilayer of liquid water and a trilayer of liquid water at $T=235$ K.[51] Owing to the large number of bulk ice phases that are observed at high pressure, water is actually the most polymorphous substance known. In this regard, it is interesting to note a recent report, using the restricted ensemble Monte Carlo method, of four supercooled bulk water liquid phases at $T=235$ K.[52]

ACKNOWLEDGMENT

This research was supported by the Soft-Link project, Contract No. 98SL010.

[1] B. Kamb, "Crystallography of ice," in *Physics and Chemistry of Ice*, edited by E. Whalley, S. J. Jones, and L. W. Gold (Royal Society of Canada, Ottawa, 1973), pp. 28–41.
[2] P. V. Hobbs, *Ice Physics* (Clarendon, Oxford, 1974).
[3] H. A. Kolodziej, B. P. Jones, and M. Davies, J. Chem. Soc., Faraday Trans. 2 **71**, 269 (1975).
[4] R. O. Watts, Chem. Phys. **57**, 185 (1981).
[5] H. E. Alper and R. M. Levy, J. Phys. Chem. **94**, 8401 (1990).
[6] M. Watanabe, A. M. Brodsky, and W. P. Reinhardt, J. Phys. Chem. **95**, 4593 (1991).
[7] A. A. Kornyshev and G. Sutmann, Phys. Rev. Lett. **79**, 3435 (1997).
[8] I.-C. Yeh and M. L. Berkowitz, J. Chem. Phys. **110**, 7935 (1999).
[9] M. Gavish, J.-L. Wang, M. Eisenstein, M. Lahav, and L. Leiserowitz, Science **256**, 815 (1992).
[10] L. Wilen, Science **259**, 1469 (1993).
[11] P. H. Poole, F. Sciortino, U. Essmann, and H. E. Stanley, Nature (London) **360**, 324 (1992).
[12] I. M. Svishchev and P. G. Kusalik, Phys. Rev. Lett. **73**, 975 (1994).

Downloaded 01 Apr 2004 to 129.125.42.3. Redistribution subject to AIP license or copyright, see http://jcp.aip.org/jcp/copyright.jsp

[13] I. M. Svishchev and P. G. Kusalik, J. Am. Chem. Soc. **118**, 649 (1996).
[14] I. M. Svishchev and P. G. Kusalik, Phys. Rev. B **53**, R8815 (1996).
[15] X. Xia and M. L. Berkowitz, Phys. Rev. Lett. **74**, 3193 (1995).
[16] I. Borzsak and P. T. Cummings, Phys. Rev. E **56**, R6279 (1997).
[17] G. Sutmann, J. Electroanal. Chem. **450**, 289 (1998).
[18] D. H. Jung, J. H. Yang, and M. S. Jhon, Chem. Phys. **244**, 331 (1999).
[19] M. Kiselev and K. Heinzinger, J. Chem. Phys. **105**, 650 (1996).
[20] A. Vegiri and S. V. Shevkunov, J. Chem. Phys. **115**, 4175 (2001).
[21] S. V. Shevkunov and A. Vegiri, J. Mol. Struct.: THEOCHEM **593**, 19 (2002).
[22] W. Drost-Hansen and J. L. Singleton, *Fundamentals of Midicinal Cell Biology*, (JAI, Greenwich, CT, 1992).
[23] J. N. Israelachvili, P. M. McGuiggan, and A. M. Homola, Science **240**, 189 (1988).
[24] S. Granick, Science **253**, 1374 (1991).
[25] J. Klein and E. Kumacheva, Science **269**, 816 (1995).
[26] R. Zangi and A. E. Mark, Phys. Rev. Lett. **91**, 025502 (2003).
[27] R. Zangi and A. E. Mark, J. Chem. Phys. **119**, 1694 (2003).
[28] E. Lindahl, B. Hess, and D. van der Spoel, J. Mol. Model. [Electronic Publication] **7**, 306 (2001).
[29] H. J. C. Berendsen, J. P. M. Postma, W. F. van Gunsteren, A. DiNola, and J. R. Haak, J. Chem. Phys. **81**, 3684 (1984).
[30] I. G. Tironi, R. Sperb, P. E. Smith, and W. F. van Gunsteren, J. Chem. Phys. **102**, 5451 (1995).
[31] M. W. Mahoney and W. L. Jorgensen, J. Chem. Phys. **112**, 8910 (2000).
[32] E. Whalley, ''The hydrogen bond in ice,'' in *The Hydrogen Bond*, edited by P. Schuster, G. Zundel, and C. Sandorfy (North-Holland, Amsterdam, 1976).
[33] S. Miyamoto and P. A. Kollman, J. Comput. Chem. **13**, 952 (1992).
[34] H. J. C. Berendsen and W. F. van Gunsteren, ''Molecular dynamics simulations: Techniques and approaches,'' in *Molecular Liquids-Dynamics and Interactions*, edited by A. J. Barnes and *et al.*, NATO ASI C 135 (Reidel, Dordrecht, The Netherlands, 1984), pp. 475–500.
[35] W. F. van Gunsteren *et al.*, *Biomolecular Simulation: GROMOS96 Manual and User Guide*, *BIOMOS b.v.* (Groningen, Zürich, 1996).
[36] A. Bondi, J. Phys. Chem. **68**, 441 (1964).
[37] K. Koga, X. C. Zeng, and H. Tanaka, Phys. Rev. Lett. **79**, 5262 (1997).
[38] L. Bosio, G. P. Johari, M. Oumezzine, and J. Teixeira, Chem. Phys. Lett. **188**, 113 (1992).
[39] F. Bruni, M. A. Ricci, and A. K. Soper, J. Chem. Phys. **109**, 1478 (1998).
[40] A. K. Soper, F. Bruni, and M. A. Ricci, J. Chem. Phys. **109**, 1486 (1998).
[41] M.-C. Bellissent-Funel, R. Sridi-Dorbez, and L. Bosio, J. Chem. Phys. **104**, 10023 (1996).
[42] Y. E. Gorbaty and Y. N. Demianets, Mol. Phys. **55**, 571 (1985).
[43] S. Neser, C. Bechinger, P. Leiderer, and T. Palberg, Phys. Rev. Lett. **79**, 2348 (1997).
[44] R. Zangi and S. A. Rice, Phys. Rev. E **61**, 660 (2000).
[45] Y. Zhu and S. Granick, Phys. Rev. Lett. **87**, 096104 (2001).
[46] U. Raviv, P. Laurat, and J. Klein, Nature (London) **413**, 51 (2001).
[47] T. Thorsen, S. J. Maerkl, and S. R. Quake, Science **298**, 580 (2002).
[48] R. Zangi and S. A. Rice, Phys. Rev. E **61**, 671 (2000).
[49] J. Frenkel, *Kinetic Theory of Liquids* (Oxford University Press, Oxford, 1946).
[50] H. E. Stanley *et al.*, Physica A **306**, 230 (2002).
[51] M. Meyer and H. E. Stanley, J. Phys. Chem. B **103**, 9728 (1999).
[52] I. Brovchenko, A. Geiger, and A. Oleinikova, J. Chem. Phys. **118**, 9473 (2003).

Downloaded 01 Apr 2004 to 129.125.42.3. Redistribution subject to AIP license or copyright, see http://jcp.aip.org/jcp/copyright.jsp